PIER

Observation of Polarization-Maintaining Near-Field Directionality

Tong Cai[1, 2, 3, #], Yuhan Zhong[2, #], Dan Liu[2, #], Hailin Huang[3],
Dengpan Wang[3], Yi Yang[4, *], Hongsheng Chen[1, 2, *], and Xiao Lin[1, 2, *]

[1]*Interdisciplinary Center for Quantum Information, State Key Laboratory of Modern Optical Instrumentation*
ZJU-Hangzhou Global Scientific and Technological Innovation Center, Zhejiang University, Hangzhou 310027, China
[2]*International Joint Innovation Center*
Key Laboratory of Advanced Micro/Nano Electronic Devices & Smart Systems of Zhejiang
The Electromagnetics Academy at Zhejiang University, Zhejiang University, Haining 314400, China
[3]*Air and Missile Defend College, Air Force Engineering University, Xi'an 710051, China*
[4]*Research Laboratory of Electronics and Department of Physics*
Massachusetts Institute of Technology, Cambridge, Massachusetts 02139, USA

ABSTRACT: Directional and highly-efficient excitation of guided waves is closely related to the on-chip information processing and is of fundamental importance to plasmonics, nanophotonics, and chiral quantum optics. However, during the directional coupling between propagating waves and guided waves, there is a loss of information about the incident polarization state. It remains elusive and challenging to preserve the incident polarization information in the near-field directionality. Here we experimentally demonstrate polarization-maintaining and polarization-dependent near-field directionality at a microwave frequency of 9.5 GHz by exploiting a reflection-free, anisotropic, and gradient metasurface. The s- and p-polarized guided waves are excited only by the s- and p-polarized components of incident waves, respectively, and they propagate predominantly to opposite designated directions. Remarkably, the measured coupling efficiency between propagating waves and guided waves exceeds 85% for arbitrary incident polarization states. Our work thus reveals a promising route to directly and efficiently convert the polarization-encoded photon qubits to polarization-encoded guided waves, a process that is highly sought after in the context of optical network and plasmonic circuitry.

1. INTRODUCTION

The optical network typically utilizes guided waves, such as surface waves at the interface between free space and metal, which are featured with a highly squeezed wavelength and a deep sub-wavelength skin depth [1–3]. As such, the optical network is promising to provide a disruptive means for the manipulation of light information at the subwavelength scale [4–7], and it finds wide applications, for example, in sensing, optical communication, optical computing, and bio-medicine [8–13].

A fundamental building block for optical networks is the excitation of guided waves on demand, including their propagation direction, coupling efficiency with the incident propagating waves, and polarization states [14–40]. Particularly, the directional coupling between propagating waves and guided waves is oftentimes regarded as a primary step towards the advanced optical network. As a result, the exotic phenomenon of near-field directionality has been extensively studied, by exploiting the quantum spin Hall effect of light [25–57] and beyond [34–37]. That is, various judiciously designed subwavelength structures (e.g., asymmetric gratings) [22–24] and complex dipolar sources (e.g., circularly polarized dipole, Huygens dipole, and Janus dipole) [14–21] have been revealed useful in
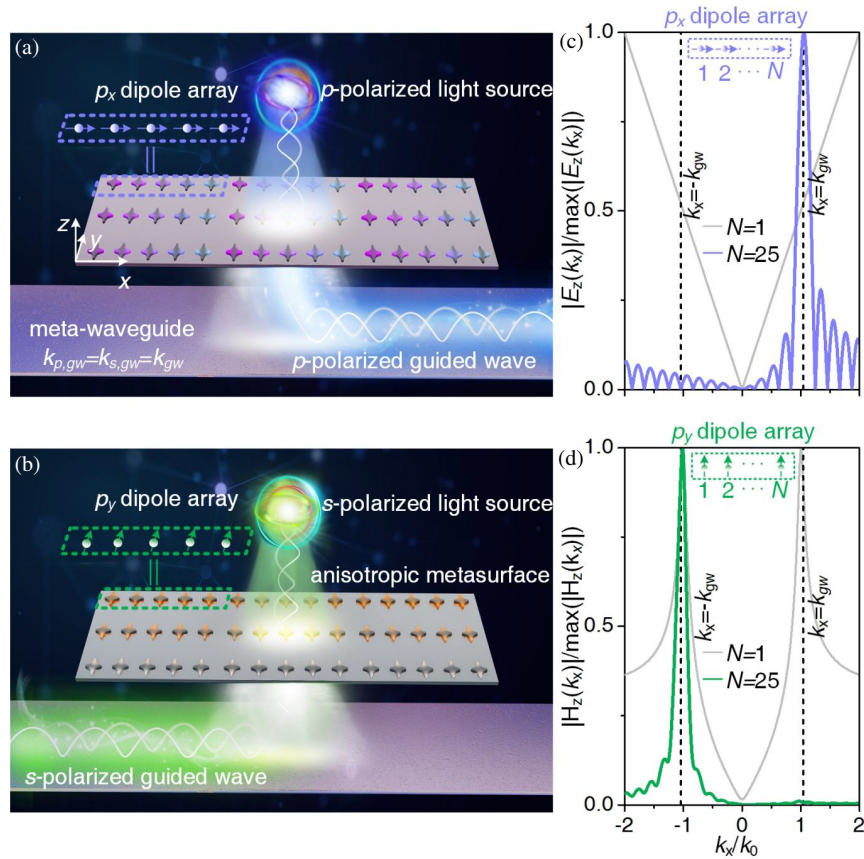
the realization of near-field directionality. Moreover, due to the recent advancement in metasurfaces, it is reported possible to achieve the high coupling efficiency between propagating waves and guided waves by using gradient metasurfaces [29–33]. Remarkably, this scheme is applicable in the near-field directionality, whose coupling efficiency can be enhanced up to 25% [32].

A next critical step for the near-field directionality is to preserve the polarization state during the coupling between propagating waves and guided waves, since the polarization of light can provide an extra degree of freedom to encode the information in optical networks. However, this polarization-maintaining near-field directionality remains un-explored especially for surface waves, partly because of the p-polarized nature of most surface waves in the optical range [22–24, 41–45]. Actually, the polarization-maintaining near-field directionality with high coupling efficiency remains elusive and an open scientific challenge, despite its importance to the further development of optical networks.

Here we propose a feasible scheme towards the polarization-maintaining near-field directionality with high coupling efficiency in a microwave regime, by depositing a reflection-free, anisotropic, and gradient metasurface close to a metawaveguide [Fig. 1]. The underlying mechanism has two folds. On the one hand, the anisotropic metasurface behaves as a p_x

---

* Corresponding authors: Xiao Lin (xiaolinzju@zju.edu.cn); Yi Yang (yiy@mit.edu); Hongsheng Chen (hansomchen@zju.edu.cn).
# These authors contributed equally.

FIGURE 1. Schematic of polarization-maintaining near-field directionality. A reflection-free, gradient, and anisotropic metasurface is deposited close to a meta-waveguide. (a), (c) Under the normal incidence of p-polarized (s-polarized) propagating waves, each supercell of the metasurface is designed to be equivalent to an N_0-element p_x (p_y) dipole array with a predefined progressive phase shift. (b), (d) Spatial frequency spectra of the phased p_x and p_y dipole arrays with $N = 5N_0$ elements. For illustration here and below, $N_0 = 5$ is used in (b), (d), the working frequency is $\omega/2\pi = 9.5$ GHz, and $k_{gw} = 1.05k_0$, where $k_0 = \omega/c$. For comparison, the spatial frequency spectra for a single dipole (i.e., $N = 1$) is also shown in (b), (d).

dipole array with a certain phase gradient under the illumination of p-polarized propagating waves, while it becomes equivalent to a p_y dipole array with the opposite phase gradient under the incidence of s-polarized propagating waves; see the schematic in Fig. 1. This way, the p-polarized (s-polarized) guided waves are excited only by the p-polarized (s-polarized) component of incident waves and would propagate predominantly to one designated (the opposite) direction, irrespective of the incident polarization state. On the other hand, the optimized metasurface-waveguide coupler can effectively suppress both the reflection at the coupling surface and the effect of the excited guided waves decoupling back into propagating waves. In our microwave experiments, the measured coupling efficiency between propagating waves and guided waves exceeds 85% for arbitrary incident polarization states.

2. RESULTS

2.1. Phased Dipole Arrays for the Polarization-Maintaining Near-Field Directionality

We begin with the analysis of the essential role of the metasurface-waveguide coupler in the polarization-

maintaining near-field directionality. Here we consider a two-dimensional case, where the guided waves propagate only along the $\pm \hat{x}$ direction [Figs. 1(a)–1(d)]. At the frequency of interest, the meta-waveguide supports both p-polarized and s-polarized guided waves with a same in-plane wavevector, namely $k_{p,gw} = k_{s,gw} = k_{gw}$; see the dispersion of guided waves in Fig. S4. The metasurface is set to be anisotropic and has a certain phase gradient along the $\hat{x}$ direction. That is, under the normal incidence of p-polarized (s-polarized) propagating waves, the metasurface is designed to be equivalent to a phased p_x (p_y) dipole array with N elements, pointing in the $\hat{x}$ ($\hat{y}$) direction and placed along the x axis with equal spacing $a = \frac{2\pi}{N_0 \cdot k_{gw}}$, where N_0 is an integer. Each dipolar element has a progressive phase shift $\alpha_p = \frac{2\pi}{N_0}$ ($\alpha_s = -\frac{2\pi}{N_0}$) relative to its adjacent element under the incidence of p-polarized (s-polarized) propagating waves.

By rigorously solving Maxwell's equations, we have $E_z(x, z) = \int E_z(k_x)e^{ik_x x}e^{ik_z|z-z_0|}dk_x$ and $H_z(x, z) = 0$ for the phased p_x dipole array in free space, where

$$E_z(k_x) = \frac{i}{8\pi^2 \varepsilon_0} k_x p_{x0} \cdot \sum_{j=1}^{N} e^{(j-1)\cdot i\left(\frac{2\pi}{N_0} - k_x a\right)} \quad (1)$$
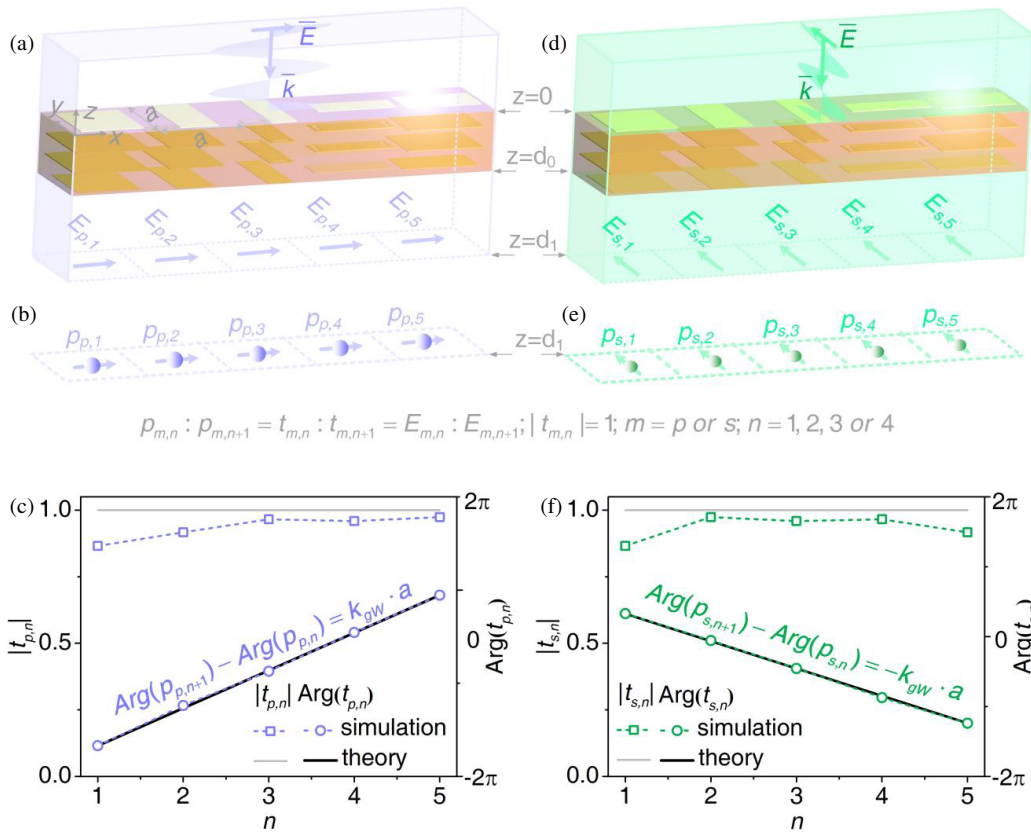
FIGURE 2. Design of reflection-free, gradient, and anisotropic metasurfaces for the polarization-maintaining near-field directionality. (a), (d) Structural schematic. Under the normal incidence of p- (s-) polarized propagating waves, the incident and transmitted electric fields are both along the $\hat{x}(\hat{y})$ direction. The transmitted electric field $E_{m,n}$ at the plane just beneath the metasurface is determined by the transmission coefficient $t_{m,n}$ of each unit cell, where m denotes the direction of electric fields and n denotes the relative position of the unit cell within a supercell of metasurface. Each supercell is set to have five unit cells. (b), (e) Modelling the transmitted electric fields by a dipole array $p_{m,n}$, where $p_{m,n} : p_{m,n+1} = E_{m,n} : E_{m,n+1} = t_{m,n} : t_{m,n+1}$. (c), (f) Transmission coefficients of the designed unit cells. For the designed transmissive metasurface, we have $|t_{m,n}| \to 1$, $\mathrm{Arg}(t_{p,n+1}) - \mathrm{Arg}(t_{p,n}) = k_{gw} \cdot a$, and $\mathrm{Arg}(t_{s,n+1}) - \mathrm{Arg}(t_{s,n}) = -k_{gw} \cdot a$. With these phase gradients, these effective dipole arrays can efficiently excite guided waves with an in-plane wavevector k_{gw}.

$k_z = \sqrt{k_0^2 - k_x^2}$, p_{x0} is the moment of each dipole, z_0 the vertical position of all dipoles in the $\hat{z}$ direction, and ε_0 the permittivity in free space [46]. By contrast, we have $E_z(x, z) = 0$ and $H_z(x, z) = \int H_z(k_x)e^{ik_x x}e^{ik_z|z-z_0|}dk_x$ for the phased p_y dipole array in free space, where

$$H_z(k_x) = \frac{i\omega}{8\pi^2} \frac{k_x p_{y0}}{k_z} \cdot \sum_{j=1}^{N} e^{(j-1)\cdot i\left(-\frac{2\pi}{N_0} - k_x a\right)} \qquad (2)$$

and p_{y0} is the moment of each dipole. Detailed derivation of $E_z(k_x, z)$ and $H_z(k_x, z)$ is given in supplementary Section S1. Since $E_z(x, z)(H_z(x, z))$ is a representative field component for p-polarized (s-polarized) waves, we can conclude that only p-polarized (s-polarized) guided waves would be excited by the phased p_x (p_y) dipole array under the illumination of p-polarized (s-polarized) propagating waves. Therefore, such a combined metasurface-waveguide coupler could well preserve the polarization state during the coupling between guided waves and propagating waves.

The spatial frequency spectra of the phased p_x and p_y dipole arrays are shown in Figs. 1(b) and 1(d), according to Equations (1)–(2). For illustration here and below, $N_0 = 5$ is used,

the frequency is $\omega/2\pi = 9.5\,\mathrm{GHz}$, and the in-plane wavevector of guided waves is $k_{gw} = 1.05k_0$, where $k_0 = \omega/c$ and c is the speed of light in free space. The ultrahigh spectral asymmetry at $k_x = \pm k_{gw}$ is achievable if N is large enough [e.g., $N = 25$ in Figs. 1(b) and 1(d)]. To be specific, we have $\frac{|E_z(k_{gw})|}{|E_z(-k_{gw})|} \gg 1$ for the p_x dipole array in Fig. 1(b) but $\frac{|H_z(k_{gw})|}{|H_z(-k_{gw})|} \ll 1$ for the p_y dipole array in Fig. 1(d). Such an ultrahigh spectral asymmetry in the k space implies the possible realization of not only polarization-maintaining but also polarization-dependent near-field directionality. That is, the directional excitation of guided waves with their polarization same as the incident propagating waves can occur; moreover, the excited guided waves with different polarizations would flow to opposite directions; see the schematic in Figs. 1(a) and 1(c).

2.2. Design of the Reflection-free, Anisotropic, and Gradient Metasurface

We now proceed to discuss a feasible design methodology for the desired metasurface in Fig. 2. Without loss of generality,
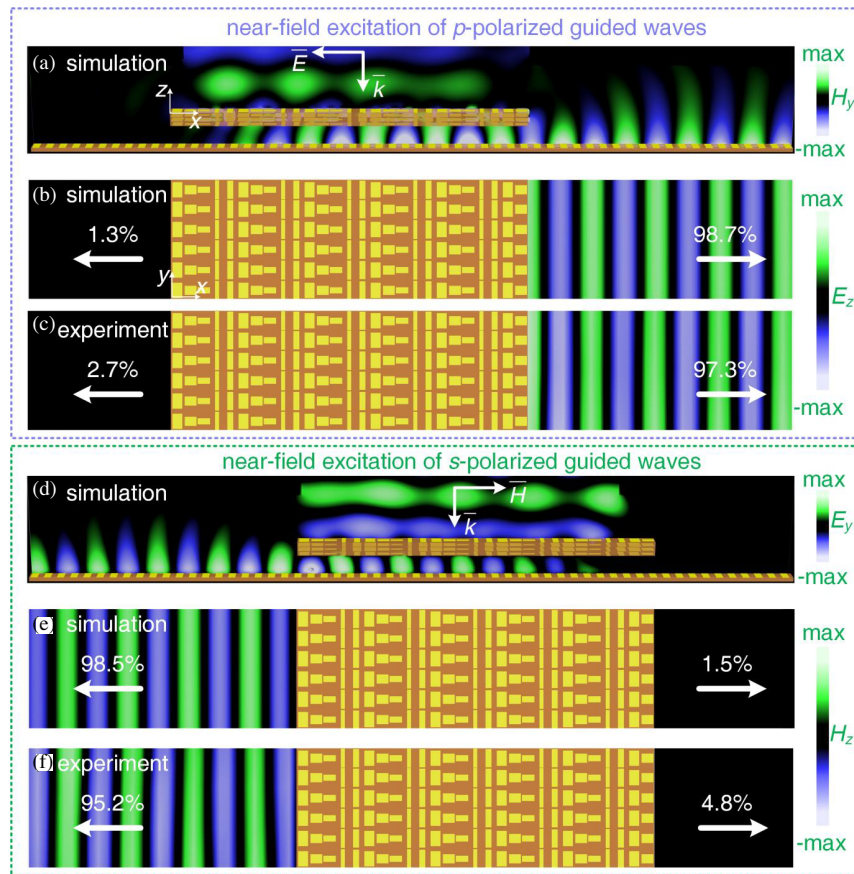
FIGURE 3. Experimental observation of the polarization-maintaining near-field directionality. (a)–(c) Under the normal incidence of p-polarized propagating waves, only p-polarized guided waves are efficiently excited, and they propagate predominantly to the right side. (d)–(f) Under the normal incidence of s-polarized propagating waves, only s-polarized guided waves are efficiently excited. By contrast, they propagate predominantly to the left side. The fields in (b), (c), (e), (f) are plotted at a plane with a distance of 10 mm above the top surface of the designed metasurface.

each supercell of metasurface has N_0 unit cells in the $\hat{x}$ direction; under the normal incidence of light, the polarization of the transmitted fields beneath each unit cell is the same as that of the incident fields [Figs. 2(a) and 2(d)], by exploiting the unique capability that anisotropic metasurface can control the transmitted fields for orthogonal polarizations independently. This way, the transmitted electric field $E_{m,n}$ beneath each unit cell is simply proportional to the corresponding transmission coefficient $t_{m,n}$, namely $E_{m,n} : E_{m,n+1} = t_{m,n} : t_{m,n+1}$, where the subscript $m = p$ or s represents the incident p-polarized or s-polarized waves, and the subscript n indicates the nth unit cell within the supercell. Due to the deep-subwavelength size of unit cells, the transmitted field beneath each unit cell can be reasonably treated as a secondary point source with a dipole moment of $p_{m,n}$ [Figs. 2(b) and 2(e)], whose orientation is dictated by the incident electric fields. In other words, we have $p_{m,n} : p_{m,n+1} = E_{m,n} : E_{m,n+1}$.

If the metasurface is reflection-free under the normal incidence of light, the corresponding transmission coefficient of each unit cell should ideally have a magnitude of unity, namely $|t_{m,n}| = 1$. Under this condition, we have $|p_{m,n}| \cdot e^{i\text{Arg}(p_{m,n})} : |p_{m,n+1}| \cdot e^{i\text{Arg}(p_{m,n+1})} = e^{i\text{Arg}(t_{m,n})} : e^{i\text{Arg}(t_{m,n+1})}$. As such, $|p_{m,n+1}| = |p_{m,n}|$ and $\text{Arg}(p_{m,n+1}) - \text{Arg}(p_{m,n}) =$

$\text{Arg}(t_{m,n+1}) - \text{Arg}(t_{m,n})$ can be obtained. Moreover, if $\text{Arg}(t_{p,n+1}) - \text{Arg}(t_{p,n}) = k_{gw} \cdot a = \alpha_p$ and $\text{Arg}(t_{s,n+1}) - \text{Arg}(t_{s,n}) = -k_{gw} \cdot a = \alpha_s$, the effective dipole arrays $p_{m,n}$ exactly correspond to the phased dipole arrays proposed in Fig. 1 with the designated progressive phase shifts. Therefore, $|t_{m,n}| = 1$ and $\text{Arg}(t_{m,n+1}) - \text{Arg}(t_{m,n}) = \alpha_m$ for each unit cell in the supercell of metasurface are actually the key conditions to enable the polarization-maintaining near-field directionality.

Due to the recent advancement in metasurfaces, these key conditions can be realized. Inspired by the isotropic ABA meta-particles [47–51], the anisotropic ABBA meta-particles can be adopted for the design of each unit cell in the metasurface, because they can enable us to achieve arbitrary transmission phases, along with a high transmission amplitude. For illustration, we show one example in Figs. 2(c) and 2(f); see the fabricated metasurface in Fig. S3. The phase condition of $\text{Arg}(t_{m,n+1}) - \text{Arg}(t_{m,n}) = \alpha_m$ is achieved, as can be seen from the perfect match between the theoretical and numerical results in Figs. 2(c) and 2(f). The magnitude condition of $|t_{m,n}| = 1$ is approximately realized, since we always have $|t_{m,n}| > 0.9$. The slight discrepancy in amplitude is mainly caused by the material loss (i.e., the material loss in the dielec-

tric). Actually, the designed anisotropic metasurface can work well within the frequency range of [9.45, 9.8] GHz in Fig. S8 and has a working bandwidth of 0.35 GHz. For illustration, below the working frequency is chosen as 9.5 GHz.

2.3. Near-Field Measurement of the Polarization-Maintaining Near-Field Directionality

The fabricated metasurface can now be combined with the judiciously designed meta-waveguide. In order to achieve the high conversion efficiency between propagating waves and guided waves, the vertical distance between the metasurface and the meta-waveguide should be optimized. Here the optimized distance is 10 mm [Fig. S5]. Based on this metasurface-waveguide coupler, we carry out the microwave measurement in Figs. 3–4. In order to clearly demonstrate the polarization-maintaining near-field directionality with high coupling efficiency, both the near-field and far-field scattering measurements are implemented.

Figure 3 shows the near-field measurement. Under the normal incidence of p-polarized propagating waves [Figs. 3(a)–3(c)], only p-polarized guided waves are efficiently excited. Moreover, 97.3% of the excited p-polarized guided waves propagates to the right side (namely $+\hat{x}$ direction). Similarly, under the normal incidence of s-polarized propagating waves [Figs. 3(d)–3(f)], only s-polarized guided waves are excited. By contrast, 95.2% of the excited s-polarized guided waves propagates to the left side ($-\hat{x}$ direction). These measured results in Figs. 3(c) and 3(f) exhibit good agreements with the numerical ones in Figs. 3(a)–(b) and 3(d)–(e), as carried out by the FDTD simulation.

2.4. Observation of the Polarization-Maintaining Near-Field Directionality with High Coupling Efficiency for Arbitrary Incident Polarization States

To quantitatively characterize the polarization-maintaining and polarization-dependent near-field directionality, Fig. 4 shows the coupling efficiency, namely the ratio between the excited power of guided waves propagating to the designated direction ($P_{p,gw,\text{right}} + P_{s,gw,\text{left}}$) and the total incident power of propagating waves ($P_{\text{incident}} = P_{p,pw} + P_{s,pw}$). Here $P_{p,pw}$ and $P_{s,pw}$ stand for the incident powers of p-polarized and s-polarized propagating waves, respectively; $P_{p,gw,\text{right}}$ ($P_{s,gw,\text{left}}$) corresponds to the excited power of the desired p-polarized (s-polarized) guided waves propagating to the designated right (left) side. For illustration, we show $P_{p,gw,\text{right}}/P_{\text{incident}}$ and $P_{s,gw,\text{left}}/P_{\text{incident}}$ in Figs. 4(a) and 4(b), respectively. Under the normal incidence of p-polarized propagating waves, we have $P_{p,gw,\text{right}}/P_{\text{incident}} = 0.88$ [Fig. 4(a)]. Similarly, we have $P_{s,gw,\text{left}}/P_{\text{incident}} = 0.86$ [Fig. 4(b)] if the incident waves are s-polarized. These measured results clearly indicate the high coupling efficiency in the observed polarization-maintaining near-field directionality.

Actually, the incident light can be arbitrarily polarized and have a random mixture of p-polarized and s-polarized propagating waves. We thus also investigate the dependence of the coupling efficiency on the incident polarization state in
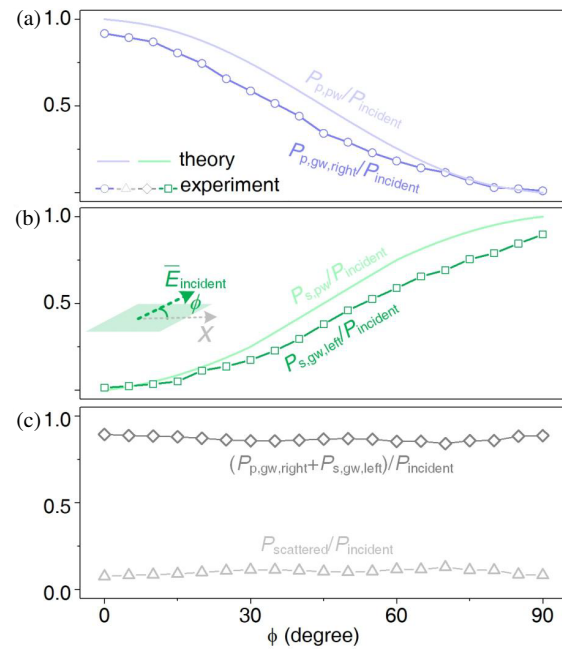
FIGURE 4. Experimental demonstration of the polarization splitting by exploiting the polarization-maintaining near-field directionality. Under normal incidence, the polarization state of incident propagating waves can be characterized by the polarization angle ϕ, namely the angle between the $\hat{x}$ direction and the total electric field $\bar{E}$. This way, $\phi = 0°$ and $\phi = 90°$ correspond to the incidence of pure p- and s-polarized propagating waves, respectively, as studied in Fig. 3. The total power of the incident propagating waves is expressed as $P_{\text{incident}} = P_{p,gw} + P_{s,gw} + P_{\text{scattered}} + P_{\text{absorption}}$, where $P_{p,gw}$ and $P_{s,gw}$ are the power of the p- and s-polarized guided wave components, respectively, $P_{\text{scattered}}$ is the power of all scattered propagating waves in the far field, and $P_{\text{absorption}}$ is the power absorbed by the coupler. $P_{s,gw,\text{left}}$ is defined as the power of the excited s-polarized guided waves propagating to the left side, while $P_{p,gw,\text{right}}$ is the power of the excited p-polarized guided waves propagating to the right side.

Figs. 4(a) and 4(b). Under the normal incidence, the incident polarization state is closely related to the angle ϕ between the direction of incident electric fields and the $\hat{x}$ direction; see the inset in Fig. 4(b). By this definition, the incident light is the p-polarized (s-polarized) propagating wave if $\phi = 0°$ ($\phi = 90°$), and the values of $P_{p,pw}/P_{\text{incident}}$ and $P_{s,pw}/P_{\text{incident}}$ would be highly dependent on ϕ as shown in Figs. 4(a) and 4(b). Remarkably, the measured $P_{p,gw,\text{right}}/P_{\text{incident}}$ as a function of ϕ almost has the same variation tendency as that of $P_{p,pw}/P_{\text{incident}}$, while the variation tendency of $P_{s,gw,\text{left}}/P_{\text{incident}}$ agrees well with that of $P_{s,pw}/P_{\text{incident}}$. Moreover, we always have $\frac{P_{p,gw,\text{right}} + P_{s,gw,\text{left}}}{P_{\text{incident}}} \geq 85\%$ [Fig. 4(c)] when ϕ changes from $0°$ to $90°$. This further indicates that the polarization-maintaining near-field directionality with high coupling efficiency can occur for arbitrary incident polarization states. This feature is also verified by the far-field measurement. From Fig. 4(c), we always have $\frac{P_{\text{scattered}}}{P_{\text{incident}}} \leq 11.2\%$ for arbitrary value of ϕ, where $P_{\text{scattered}}$ stands for all scattered power into propagating waves; see the calculation in Fig. S6. In addition, a minor proportion of power (around 2%) would be dissipated during the coupling, due to the material loss in the designed metasurface.

3. CONCLUSION

In summary, we have theoretically proposed and experimentally demonstrated the polarization-maintaining near-field directionality with high coupling efficiency, by exploiting a judiciously designed metasurface-waveguide coupler. This exotic near-field directionality is independent of the handedness of circularly polarized light but becomes dependent on the polarization of linearly polarized light. Moreover, while the high far-to-near-field coupling efficiency is insensitive to the incident polarization state, engineering the incident polarization state can continuously tune not only the directionality but also the polarization of the excited guided waves. Our work thus demonstrates a promising route to maintain the polarization state during the far-to-near field coupling and to spatially separate the incident information with different linear polarizations. In conjunction with the dynamic polarization modulation technique, this exotic polarization-maintaining near-field directionality would enable an enticing capability to encode the polarization information into the guided waves. Such a capability may help to further harness the unique feature of guided waves for wide applications in the classic and quantum information communication and may promote the further development of the optical network and the plasmonic circuitry.

REFERENCES

[1] Bogaerts, W., D. Pérez, J. Capmany, D. A. B. Miller, J. Poon, D. Englund, F. Morichetti, and A. Melloni, "Programmable photonic circuits," *Nature*, Vol. 586, No. 7828, 207–216, Oct. 2020.

[2] Tame, M. S., K. R. McEnery, S. K. Özdemir, J. Lee, S. A. Maier, and M. S. Kim, "Quantum plasmonics," *Nature Physics*, Vol. 9, No. 6, 329–340, Jun. 2013.

[3] Yu, N. and F. Capasso, "Flat optics with designer metasurfaces," *Nature Materials*, Vol. 13, No. 2, 139–150, Jan. 2014.

[4] Gong, S.-H., F. Alpeggiani, B. Sciacca, E. C. Garnett, and L. Kuipers, "Nanoscale chiral valley-photon interface through optical spin-orbit coupling," *Science*, Vol. 359, No. 6374, 443–447, Jan. 2018.

[5] Chen, J., X. Lin, M. Chen, T. Low, H. Chen, and S. Dai, "A perspective of twisted photonic structures," *Applied Physics Letters*, Vol. 119, No. 24, 240501, Dec. 2021.

[6] Söllner, I., S. Mahmoodian, S. L. Hansen, L. Midolo, A. Javadi, G. Kiršanskė, T. Pregnolato, H. El-Ella, E. H. Lee, J. D. Song, S. Stobbe, and P. Lodahl, "Deterministic photon-emitter coupling in chiral photonic circuits," *Nature Nanotechnology*, Vol. 10, No. 9, 775–778, Jul. 2015.

[7] Shen, L., X. Lin, M. Y. Shalaginov, T. Low, X. Zhang, B. Zhang, and H. Chen, "Broadband enhancement of on-chip single-photon extraction via tilted hyperbolic metamaterials," *Applied Physics Reviews*, Vol. 7, No. 2, 021403, Jun. 2020.

[8] Mitsch, R., C. Sayrin, B. Albrecht, P. Schneeweiss, and A. Rauschenbeutel, "Quantum state-controlled directional spontaneous emission of photons into a nanophotonic waveguide," *Nature Communications*, Vol. 5, No. 1, 5713, Dec. 2014.

[9] Xu, J.-S., M.-H. Yung, X.-Y. Xu, J.-S. Tang, C.-F. Li, and G.-C. Guo, "Robust bidirectional links for photonic quantum networks," *Science Advances*, Vol. 2, No. 1, e1500672, Jan. 2016.

[10] Antikainen, A., R.-J. Essiambre, and G. P. Agrawal, "Determination of modes of elliptical waveguides with ellipse transformation perturbation theory," *Optica*, Vol. 4, No. 12, 1510–1513, Dec. 2017.

[11] Zheng, X., J. Lin, Z. Wang, H. Zhou, Q. He, and L. Zhou, "Manipulating light transmission and absorption via an achromatic reflectionless metasurface," *PhotoniX*, Vol. 4, No. 1, 3, Jan. 2023.

[12] Kim, J. H., J. Y. Lee, E. S. Kim, and M. Y. Jeong, "Electric field enhancement of coupled plasmonic nanostructures for optical amplification," *PhotoniX*, Vol. 4, No. 1, 8, Feb. 2023.

[13] Wang, C., X. Chen, Z. Gong, R. Chen, H. Hu, H. Wang, Y. Yang, L. Tony, B. Zhang, H. Chen, and X. Lin, "Superscattering of light: Fundamentals and applications," *Reports on Progress in Physics*, Vol. 87, No. 12, 126401, Nov. 2024.

[14] Chen, X., C. Wang, Y. Zhong, B. Zhang, H. Chen, and X. Lin, "Dipolar Huygens-Kerker radiation for surface waves," *Optics Letters*, Vol. 49, No. 15, 4238–4241, Jul. 2024.

[15] Bian, C., Y. Zhong, X. Chen, T. Low, H. Chen, B. Zhang, and X. Lin, "Janus faces of dipolar sources in directional near-field coupling with an oriented misalignment," *Physical Review A*, Vol. 109, No. 3, 033505, Mar. 2024.

[16] Rodríguez-Fortuño, F. J., G. Marino, P. Ginzburg, D. O'Connor, *et al.*, "Near-field interference for the unidirectional excitation of electromagnetic guided modes," *Science*, Vol. 340, No. 6130, 328–330, Apr. 2013.

[17] Picardi, M. F., A. Manjavacas, A. V. Zayats, and F. J. Rodríguez-Fortuño, "Unidirectional evanescent-wave coupling from circularly polarized electric and magnetic dipoles: An angular spectrum approach," *Physical Review B*, Vol. 95, No. 24, 245416, Jun. 2017.

[18] Long, Y., J. Ren, Z. Guo, H. Jiang, Y. Wang, Y. Sun, and H. Chen, "Designing all-electric subwavelength metasources for near-field photonic routings," *Physical Review Letters*, Vol. 125, No. 15, 157401, Oct. 2020.

[19] Zhong, Y., X. Lin, J. Jiang, Y. Yang, G.-G. Liu, H. Xue, T. Low, H. Chen, and B. Zhang, "Toggling near-field directionality via polarization control of surface waves," *Laser & Photonics Reviews*, Vol. 15, No. 4, 2000388, Feb. 2021.

[20] Wang, M., H. Zhang, T. Kovalevich, R. Salut, M.-S. Kim, M. A. Suarez, M.-P. Bernal, H.-P. Herzig, H. Lu, and T. Grosjean, "Magnetic spin-orbit interaction of light," *Light: Science & Applications*, Vol. 7, No. 1, 24, Jun. 2018.

[21] Picardi, M. F., A. V. Zayats, and F. J. Rodríguez-Fortuño, "Not every dipole is the same: The hidden patterns of dipolar near fields," *Europhysics News*, Vol. 49, No. 4, 14–18, Sep. 2018.

[22] Zang, T., H. Zang, Z. Xi, J. Du, H. Wang, Y. Lu, and P. Wang, "Asymmetric excitation of surface plasmon polaritons via paired slot antennas for angstrom displacement sensing," *Physical Review Letters*, Vol. 124, No. 24, 243901, Jun. 2020.

[23] López-Tejeira, F., S. G. Rodrigo, L. Martín-Moreno, F. J. García-Vidal, E. Devaux, T. W. Ebbesen, J. R. Krenn, I. P. Radko, S. I. Bozhevolnyi, M. U. González, J. C. Weeber, and A. Dereux, "Efficient unidirectional nanoslit couplers for surface plasmons," *Nature Physics*, Vol. 3, No. 5, 324–328, Apr. 2007.

[24] Cheng, Q., Y. Pan, H. Wang, C. Zhang, D. Yu, A. Gover, H. Zhang, T. Li, L. Zhou, and S. Zhu, "Observation of anomalous π modes in photonic floquet engineering," *Physical Review Letters*, Vol. 122, No. 17, 173901, May 2019.

[25] Bliokh, K. Y., D. Smirnova, and F. Nori, "Quantum spin hall effect of light," *Science*, Vol. 348, No. 6242, 1448–1451, Jun. 2015.

[26] Bliokh, K. Y., F. J. Rodríguez-Fortuño, F. Nori, and A. V. Zayats, "Spin-orbit interactions of light," *Nature Photonics*, Vol. 9, No. 12, 796–808, Nov. 2015.

[27] Van Mechelen, T. and Z. Jacob, "Universal spin-momentum locking of evanescent waves," *Optica*, Vol. 3, No. 2, 118–126, Jan. 2016.

[28] Kapitanova, P. V., P. Ginzburg, F. J. Rodríguez-Fortuño, D. S. Filonov, P. M. Voroshilov, P. A. Belov, A. N. Poddubny, Y. S. Kivshar, G. A. Wurtz, and A. V. Zayats, "Photonic spin Hall effect in hyperbolic metamaterials for polarization-controlled routing of subwavelength modes," *Nature Communications*, Vol. 5, No. 1, 3226, Feb. 2014.

[29] Sun, S., Q. He, S. Xiao, Q. Xu, X. Li, and L. Zhou, "Gradient-index meta-surfaces as a bridge linking propagating waves and surface waves," *Nature Materials*, Vol. 11, No. 5, 426–431, Apr. 2012.

[30] Cai, T., S. Tang, G. Wang, H. Xu, S. Sun, Q. He, and L. Zhou, "High-performance bifunctional metasurfaces in transmission and reflection geometries," *Advanced Optical Materials*, Vol. 5, No. 2, 1600506, Jan. 2017.

[31] Sun, W., Q. He, S. Sun, and L. Zhou, "High-efficiency surface plasmon meta-couplers: Concept and microwave-regime realizations," *Light: Science & Applications*, Vol. 5, No. 1, e16003, Jan. 2016.

[32] Pors, A., M. G. Nielsen, T. Bernardin, J.-C. Weeber, and S. I. Bozhevolnyi, "Efficient unidirectional polarization-controlled excitation of surface plasmon polaritons," *Light: Science & Applications*, Vol. 3, No. 8, e197, Aug. 2014.

[33] Wang, Z., S. Li, X. Zhang, X. Feng, Q. Wang, J. Han, Q. He, W. Zhang, S. Sun, and L. Zhou, "Excite spoof surface plasmons with tailored wavefronts using high-efficiency terahertz metasurfaces," *Advanced Science*, Vol. 7, No. 19, 2000982, Oct. 2020.

[34] Picardi, M. F., A. V. Zayats, and F. J. Rodríguez-Fortuño, "Amplitude and phase control of guided modes excitation from a single dipole source: Engineering far- and near-field directionality," *Laser & Photonics Reviews*, Vol. 13, No. 12, 1900250, Nov. 2019.

[35] Shi, X., X. Lin, I. Kaminer, F. Gao, Z. Yang, J. D. Joannopoulos, M. Soljačić, and B. Zhang, "Superlight inverse Doppler effect," *Nature Physics*, Vol. 14, No. 10, 1001–1005, Jul. 2018.

[36] Lin, X. and B. Zhang, "Normal Doppler frequency shift in negative refractive-index systems," *Laser & Photonics Reviews*,

Vol. 13, No. 12, 1900081, Nov. 2019.

[37] Picardi, M. F., A. V. Zayats, and F. J. Rodríguez-Fortuño, "Janus and Huygens dipoles: Near-field directionality beyond spin-momentum locking," *Physical Review Letters*, Vol. 120, No. 11, 117402, Mar. 2018.

[38] Wang, C., Y. Zhong, X. Chen, H. Wang, T. Low, H. Chen, B. Zhang, and X. Lin, "Near-field coupling of Janus dipoles beyond polarization locking," *Laser & Photonics Reviews*, Vol. 18, No. 10, 2301035, Oct. 2024.

[39] Ma, W., X. Chen, Y. Zhong, C. Bian, C. Wang, H. Chen, and X. Lin, "Toggling near-field directionality via manipulation of matter's anisotropy," *Optics Letters*, Vol. 49, No. 20, 5862–5865, Oct. 2024.

[40] Zhong, Y., C. Wang, C. Bian, X. Chen, J. Chen, X. Zhu, H. Hu, T. Low, H. Chen, B. Zhang, and X. Lin, "Near-field directionality governed by asymmetric dipole-matter interactions," *Optics Letters*, Vol. 49, No. 4, 826–829, Feb. 2024.

[41] Lin, J., J. P. B. Mueller, Q. Wang, G. H. Yuan, N. Antoniou, X. C. Yuan, and F. Capasso, "Polarization-controlled tunable directional coupling of surface plasmon polaritons," *Science*, Vol. 340, No. 6130, 331–334, Apr. 2013.

[42] Kuznetsov, A. I., A. E. Miroshnichenko, M. L. Brongersma, Y. S. Kivshar, and B. Luk'yanchuk, "Optically resonant dielectric nanostructures," *Science*, Vol. 354, No. 6314, aag2472, Nov. 2016.

[43] O'connor, D., P. Ginzburg, F. J. Rodríguez-Fortuño, G. A. Wurtz, and A. V. Zayats, "Spin-orbit coupling in surface plasmon scattering by nanostructures," *Nature Communications*, Vol. 5, No. 1, 5327, Nov. 2014.

[44] Zhang, Y., Y. Luo, Y. Zhang, Y.-J. Yu, Y.-M. Kuang, L. Zhang, Q.-S. Meng, Y. Luo, J.-L. Yang, Z.-C. Dong, and J. G. Hou, "Visualizing coherent intermolecular dipole-dipole coupling in real space," *Nature*, Vol. 531, No. 7596, 623–627, Mar. 2016.

[45] Petersen, J., J. Volz, and A. Rauschenbeutel, "Chiral nanophotonic waveguide interface based on spin-orbit interaction of light," *Science*, Vol. 346, No. 6205, 67–71, Sep. 2014.

[46] Kong, J. A., *Electromagnetic Waves Theory*, EMW Publishing, Cambridge, MA, 2008.

[47] Cai, T., G. M. Wang, S. W. Tang, H. X. Xu, J. W. Duan, H. J. Guo, F. X. Guan, S. L. Sun, Q. He, and L. Zhou, "High-efficiency and full-space manipulation of electromagnetic wave fronts with metasurfaces," *Physical Review Applied*, Vol. 8, No. 3, 034033, Sep. 2017.

[48] Pfeiffer, C. and A. Grbic, "Metamaterial Huygens' surfaces: Tailoring wave fronts with reflectionless sheets," *Physical Review Letters*, Vol. 110, No. 19, 197401, May 2013.

[49] Achouri, K. and C. Caloz, "Design, concepts, and applications of electromagnetic metasurfaces," *Nanophotonics*, Vol. 7, No. 6, 1095–1116, May 2018.

[50] Lavigne, G., K. Achouri, V. S. Asadchy, S. A. Tretyakov, and C. Caloz, "Susceptibility derivation and experimental demonstration of refracting metasurfaces without spurious diffraction," *IEEE Transactions on Antennas and Propagation*, Vol. 66, No. 3, 1321–1330, Mar. 2018.

[51] Jia, M., Z. Wang, H. Li, X. Wang, W. Luo, S. Sun, Y. Zhang, Q. He, and L. Zhou, "Efficient manipulations of circularly polarized terahertz waves with transmissive metasurfaces," *Light: Science & Applications*, Vol. 8, No. 1, 16, Jan. 2019.